JACS
JOURNAL OF THE AMERICAN CHEMICAL SOCIETY
pubs.acs.org/JACS

Article

Synthesis, Structure, and Electronic Properties of $[Cr_6@Sn_8Sb_8(en)_2]^{3-}$: A Cr_6 Octahedron Encapsulated in a Zintl-Ion Ligand

Wei-Xing Chen,[§] Aidan Manley,[§] Zi-Sheng Li, John E. McGrady,* and Zhong-Ming Sun*

Cite This: J. Am. Chem. Soc. 2025, 147, 24309−24316

Read Online

ACCESS | Metrics & More | Article Recommendations | Supporting Information

ABSTRACT: The reaction of $CrCp_2$ with K_2SnSb yields a Zintl-ion cluster containing an octahedral Cr_6 core, surrounded by an Sn_8Sb_8 ring and two further ethylenediamine ligands that cap two mutually *trans* Cr centers. The Cr−Cr bond lengths of 2.453(2) to 2.482(2) Å are remarkably short, much shorter than those in any of the 20-electron chalcogenide-capped analogues, $Cr_6E_8(PR_3)_6$, indicating unusually strong Cr−Cr bonding. An isotropic signal in the electron paramagnetic resonance (EPR) spectrum with g = 2.21 is consistent with a 23-electron Cr_6^{13+} core, three electrons more reduced than the Cr_6^{16+} units present in $Cr_6E_8(PR_3)_6$. An analysis of the electronic structure using density functional theory (DFT) indicates that the additional three electrons enter Cr−Cr bonding orbitals, which are stabilized as a result of the weak π-donor properties of the $Sn_8Sb_8^{16-}$ Zintl ligand.

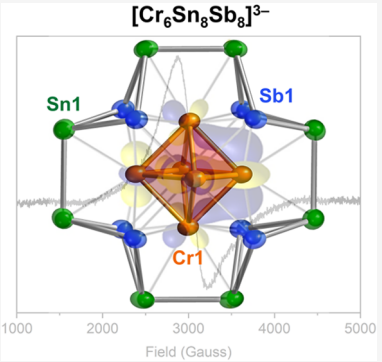

INTRODUCTION

The elements of group 6, chromium molybdenum and tungsten, have played a central part in the history of the metal−metal bond,[1,2] beginning with the first report of $Cr_2(CH_3COO)_4(H_2O)_2$ by Peligot,[3] a dimer that was shown, over a century later, to contain a Cr−Cr quadruple bond.[4,5] More recently, the use of alkali metal reducing agents has given access to a range of Cr^I species linked by quintuple bonds, exemplified by Power's 2005 discovery of *trans*-bent $Cr_2Ar'_2$, Ar' = C_6H_3-2,6-(C_6H_3-2,6-($CHMe_2$)$_2$)$_2$ (Figure 1a).[6,7] Larger clusters containing three or more Cr atoms are also well established, notably in Betley's trichromium complex (^{tbs}L)-Cr_3(thf), which shows promise in small molecule activation (Figure 1b).[8] The coordination spheres of the clusters described above are completed by traditional inorganic and organometallic ligands such as amides, sulfides, phosphines, and alkyl groups, but alternative ligand architectures made up of circular or spherical arrays of *p*-block (semi)metal atoms such as Ge, Sn, As, Sb ("Zintl ions") are emerging as alternative scaffolds for stabilizing metal ions and clusters.[9−11] Notable recent examples include $[Fe@Ge_{10}]^{3-}$,[12] $[Ru@Ge_{12}]^{3-}$,[13] $[Ln@Sb_{12}]^{3-}$ (Ln = La, Y, Ho, Er, Lu),[14] and $[An@Bi_{12}]^{n-}$ (An/n = U/3; Th/4)[15,16] (Figure 1d), where we use @ to indicate endohedral encapsulation. The structures of the last two molecules in this list highlight the important principle that cyclic arrays made up of three butterfly Pn_4 units can span the circumference of relatively large metal cations. There are rather fewer examples where a cluster of three or more transition metals, as distinct from an isolated atom, is encapsulated within a Zintl core, but the $[Pd_3Sn_8Bi_6]^{4-}$ cluster (Figure 1e) was reported by Dehnen and co-workers.[17] In a very recent publication, we have shown that a low-valent Cr precursor, $CrCp_2$, reacts with the Sb-rich Zintl phase K_8SnSb_4 to form a pentagonal Cr_5 cluster, $[Cr_5Sb_{20}Sn_2]^{4-}$, with very short Cr−Cr bonds (2.539− 2.625 Å) encapsulated by an Sb_{20} ring made up of five fused Sb_4 units.[18] Extrapolating from $[Ln@Sb_{12}]^{3-}$, it seems that cyclic arrays based on Pn_4 units (or their isoelectronic analogues) may therefore provide a versatile platform for encapsulating clusters of different sizes. Inspired by this hypothesis, we now report our attempts to use a more Sn-rich Zintl phase, K_2SnSb, as a Pn_4 surrogate to construct chromium cluster compounds. The pseudoelement concept establishes an equivalence between Sb and Sn^-, so increasing Sn content should increase the net negative charge on the main group component, which may, in turn, stabilize a more highly oxidized Cr core than the one present in $[Cr_5Sb_{20}Sn_2]^{4-}$. We show here that the reaction of K_2SnSb with $CrCp_2$ leads to a new Zintl cluster, $[Cr_6@Sn_8Sb_8(en)_2]^{3-}$ (Figure 1f), containing an octahedral Cr_6 core encapsulated in a Zintl-ion ring made up of four fused Sn_2Sb_2 units. The Cr−Cr bond lengths are substantially shorter than those in the $Cr_6E_8(PR_3)_6$ family (Figure 1c), a well-established structural motif across the

Received: January 10, 2025
Revised: June 24, 2025
Accepted: June 25, 2025
Published: July 8, 2025

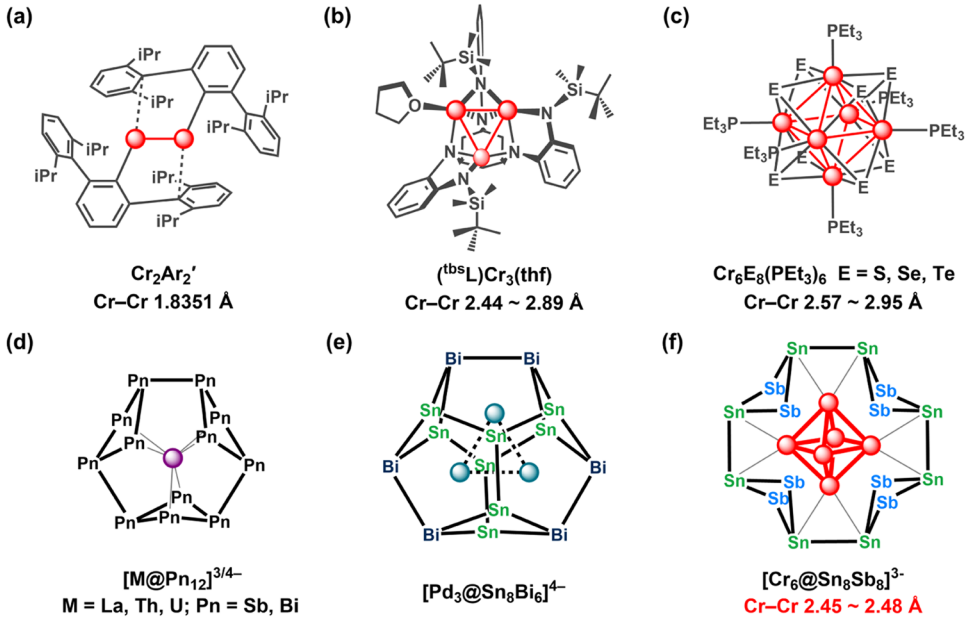

Figure 1. Examples of clusters stabilized by classic ligand sets (a–c) and by cyclic "Zintl" arrays of *p*-block elements (d–f).

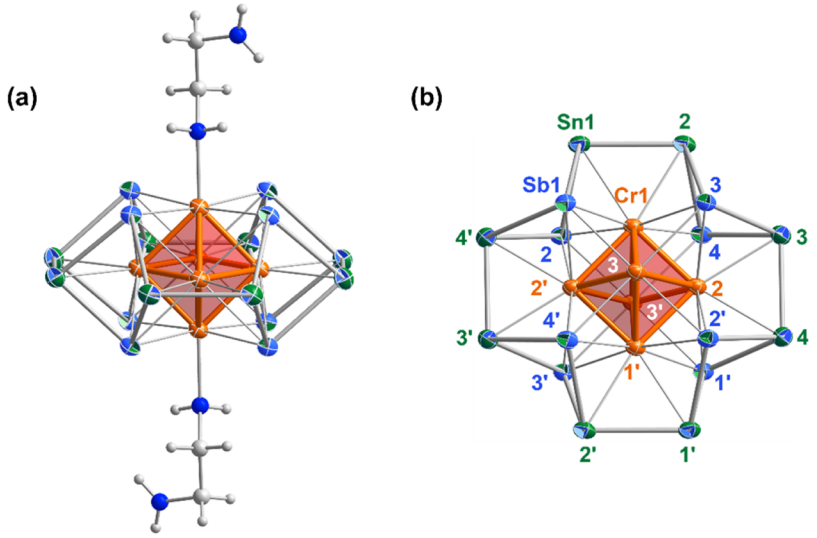

Figure 2. Molecular structure of $[Cr_6@Sn_8Sb_8(en)_2]^{3-}$ with 50% probability ellipsoids, viewed (a) perpendicular to and (b) along the approximate 4-fold rotational axis. As Sn and Sb cannot be distinguished by X-ray crystallography, these atoms are displayed as two-color octants, with the outer color representing the more likely atom type at each atomic position based on our density functional theory (DFT) calculations (*vide infra*). The two en ligands are omitted from the second view for clarity.

majority of the transition block.[19−26] In addition to characterization through X-ray crystallography and electron paramagnetic resonance (EPR) spectroscopy, we use density functionals to explore the electronic structure of this new cluster and establish its place in the context of the extended octahedral M_6 family.

RESULTS AND DISCUSSION

Synthesis and Structure. $\{[K(18\text{-C-}6)]_2Cp\}_3\{[Cr_6@Sn_8Sb_8(en)_2]\}$ (**1**) was prepared by reacting an ethylenediamine (en) solution of the ternary Zintl precursor K_2SnSb with $CrCp_2$ in the presence of 18-crown-6 at room temperature. Full details of the synthesis are given in the Experimental Section. **1** crystallizes in the triclinic space group $P\bar{1}$, and the unit cell contains a single $[Cr_6@Sn_8Sb_8(en)_2]^{3-}$ anion as well as six K^+ cations, three of which are bound to Cp^- ligands derived from the $CrCp_2$ starting material (Figure 2a and Supporting Information, Figures S1–S3). Important bond lengths are collected in Table 1. The formulation of the cluster as a trianion, $[Cr_6@Sn_8Sb_8(en)_2]^{3-}$, requires that it is paramagnetic, and indeed, the electron paramagnetic resonance (EPR) spectrum measured at 95 K, shown in Figure 3, shows a broad anisotropic signal centered at g = 2.21. The $Cr_6@Sn_8Sb_8$ core of the cluster has approximate D_{4h} symmetry, with four Cr atoms in the equatorial plane surrounded by a Sn_8Sb_8 ring. The remaining two Cr atoms bind in the axial positions and are terminated by en ligands, which are bound via a single nitrogen atom. All 12 Cr–Cr bond lengths are below 2.5 Å, with those in the equatorial plane marginally shorter, at ~2.46 Å, than those between equatorial and axial Cr

https://doi.org/10.1021/jacs.5c00515
J. Am. Chem. Soc. 2025, 147, 24309−24316

Table 1. Summary of X-ray Data and Relative Energies (eV) and Selected Bond Lengths (All in Å) for the $^2A_1$ and $^2B_1$ States of $[Cr_6@Sn_8Sb_8(en)_2]^{3-}$[a]

		E/eV	Cr_{eq}–Cr_{eq}	Cr_{eq}–Cr_{ax}	Cr_{eq}–Sb	Cr_{ax}–Sb	Cr_{eq}–Sn	Sn–Sn	Sn–Sb	references
X-ray			2.453(2)–2.457(1)	2.480(2)–2.482(2)	2.739(2)–2.754(2)	2.778(1)–2.790(1)	2.787(1)–2.809(2)	2.9353(9)–2.9293(7)	2.9106(8)–2.9262(8)	this work
DFT	$^2A_1$ (Sn radical)	0.00	2.39	2.42	2.78–2.79	2.78–2.80	2.89–2.91	3.04–3.05	2.97–2.98	
	$^2B_1$ (Cr_6 radical)	+0.03	2.44–2.45	2.36–2.47	2.78–2.80	2.81–2.85	2.85–2.93	2.96–2.99	2.96–2.99	
							Cr–P			
	$Cr_6E_8(PEt_3)_6$		Cr–Cr		Cr–E					
	$Cr_6S_8(PEt_3)_6$		2.59–2.60		2.33–2.35		2.39–2.42			26
	$Cr_6Se_8(PEt_3)_6$		2.67–2.71		2.43–2.45		2.41–2.43			26
	$Cr_6Te_8(PEt_3)_6$		2.82–2.86		2.65–2.67		2.43–2.45			26

[a]A structural comparison to members of the $Cr_6E_8(PR_3)_6$ family is shown in the lower half of the table.

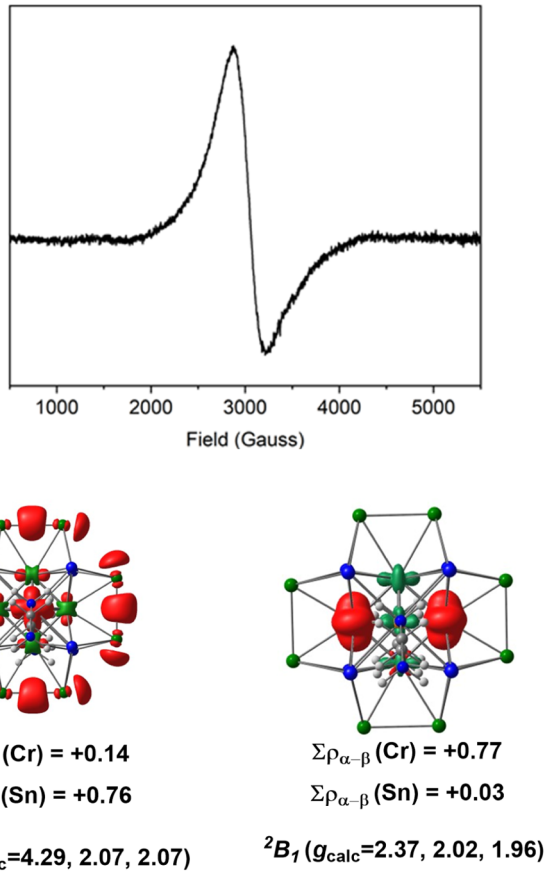

Figure 3. X-band (9.3943 GHz) EPR spectrum of a crystalline sample of **1** in DMF and net spin densities for the $^2A_1$ ("Sn radical") and $^2B_1$ ("Cr_6 radical") states of $[Cr_6@Sn_8Sb_8(en)_2]^{3-}$. Contour values for the isosurface plots are 0.001 e/au^3.

atoms (~2.48 Å). These values are intermediate between those in the recently characterized $[Cr_3Sn_2Sb_{20}]^{4-}$ cluster (2.59–2.62 Å)[18] and the $[Cr_2Sb_{12}]^{3-}$ dimer (2.319 Å), where significant Cr–Cr multiple bonding is present.[27] The Cr–Cr bonds in **1** are also strikingly shorter than those in any of the Cr_6 chalcogenides, $Cr_6E_8(PR_3)_6$ (also collected in Table 1).[19−26] The most direct comparison is to the telluride, $Cr_6Te_8(PR_3)_6$ (because Te is in the same period as Sn and Sb), and there the average Cr–Cr bond length is in excess of 2.80 Å. The Cr–Cr bonding in **1** appears, therefore, to stand out as being much stronger than in comparable Cr_6 octahedra.

It is important to acknowledge that we are not able to distinguish Sn from Sb in the diffraction data because their atomic numbers differ by only one − this is a common problem in Zintl cluster chemistry where elements from groups 14 and 15 of the same period are present.[28,29] However, an 8:8 Sn/Sb ratio in the product is supported by energy dispersive X-ray (EDX) analysis (Supporting Information, Figure S4), where the measured ratio is 7.9:8.4. From this data alone, we cannot absolutely exclude an alternative 7:9 formulation, but given that the X-ray structure places the period 5 elements (Sn/Sb) in two quite different crystallographic positions in an 8:8 ratio, this seems the most likely formulation. ESI mass spectrometry performed on freshly prepared samples of **1** in DMF solution (Supporting Information, Figures S5 and S6) shows evidence for extensive fragmentation, as is commonly observed in Zintl cluster chemistry. There is, however, a small peak at m/z 1401.8384 that could be assigned to the dianion

https://doi.org/10.1021/jacs.5c00515
J. Am. Chem. Soc. 2025, 147, 24309−24316

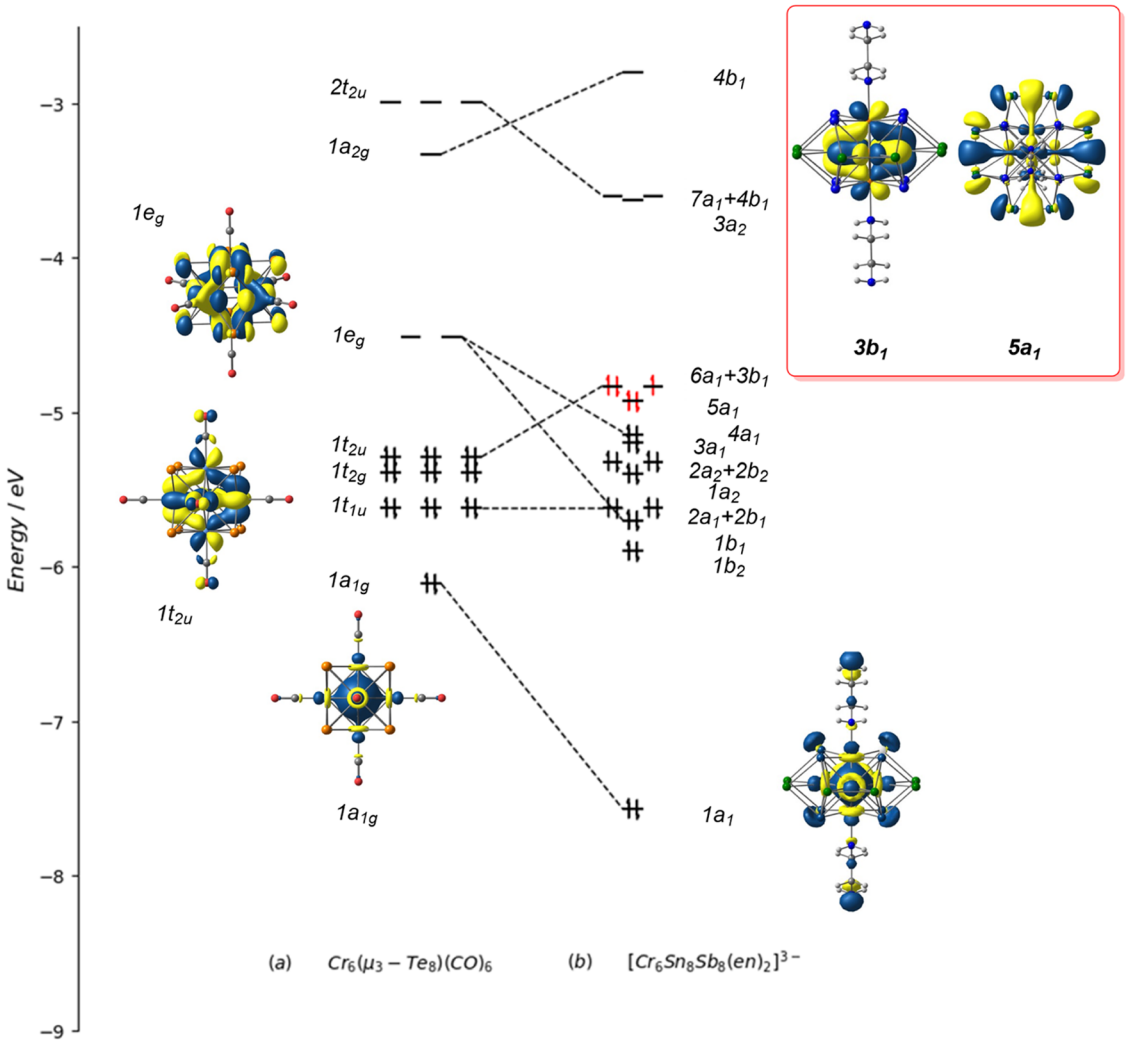

Figure 4. Comparison of the frontier orbitals of (a) $Cr_6Te_8(CO)_6$ and (b) $[Cr_6@Sn_8Sb_8(en)_2]^{3-}$. The orbitals of the latter have been grouped to emphasize the degeneracies that are present in the D_{4h} limit. Contour values for the isosurface plots are 0.025 $e^{1/2}/au^{3/2}$.

$[\{[K(18\text{-}C\text{-}6)]_2Cp\}Sn_8Sb_8Cr_4]^{2-}$, again consistent with an 8:8 ratio of Sn to Sb. These data are discussed in more detail in the Supporting Information.

In order to establish the precise positions of Sn and Sb within the cluster, we have turned to density functional theory (DFT) to identify the most stable arrangements of atoms. A systematic survey of all possible permutations of Sn and Sb in **1** is beyond the scope of this paper, but we have separately optimized geometries for four distinct models including the one shown in Figure 2 where the Sn atoms lie in the equatorial plane, and the Sb atoms cap the eight triangular faces of the Cr_6 octahedron. We have also considered an alternative where the positions are reversed (Sb atoms in the equatorial plane and Sn in the face-capping sites), another where half of the Sn and Sb are swapped, and a third where a single Sb is present in the equatorial plane and a single Sn in one of the capping sites. Details are collected in the Supporting Information, Figure S7, but the first of the above arrangements, with all eight Sn atoms in the equatorial plane and all eight Sb in the face-capping positions, proves to be significantly more stable than any of the alternatives, and the match to the experimental bond lengths is also the best. To reflect the ambiguity over the positions of the Sn and Sb atoms, they are displayed as two-color octants in Figure 2, with the outer color representing the atom at that site in the most stable computed structure. With the positions of the Sb and Sn atoms established, we can confirm that the average Cr−Sn (2.798 Å) and Cr−Sb (2.760 Å) bond lengths in **1** are fully consistent with those in known organometallic compounds such as $R_3SnCr(CO)_3C_5Me_5$ (R = Ph, Cy); Cr−Sn = 2.765 Å, (av.)[30] and $(ArSb)Cr(CO)_5$; Sb−Cr = 2.748 Å[31] but marginally shorter than those in Zintl cluster anions such as $[Sn_9Cr(CO)_3]^{4-}$; Cr−Sn = 2.864 Å[32] and $[Sb_7Cr(CO)_3]^{3-}$; Cr−Sb = 2.827 Å.[33] Sn−Sn bond lengths of 2.93 Å are marginally longer than those in the isolated $(Sn_2Sb_2)^{2-}$ anion (2.852−2.884 Å),[29] but very similar to those in $[Pd_3Sn_8Bi_6]^{4-}$ (2.91 Å).[17] In the context of the following discussion of the electronic structure, it is also significant that the Cr−Sb bond lengths are much longer than the corresponding Cr−Te bonds in $Cr_6Te_8(PR_3)_6$ (ca. 2.64 Å).

Electronic Structure. Density functional theory has been used to explore the potential energy surface of the cluster anion, $[Cr_6@Sn_8Sb_8(en)_2]^{3-}$, with the aim of establishing (a) the identity of the electronic ground state and (b) the origin of the very short Cr−Cr bonds. In the X-ray structure, the $Cr_6@Sn_8Sb_8$ core has approximate D_{4h} symmetry, but the internal structure of the en ligands precludes the use of such high symmetry in the actual calculations. The conformation of the en ligands has therefore been selected to give the highest

https://doi.org/10.1021/jacs.5c00515
J. Am. Chem. Soc. 2025, 147, 24309−24316

possible symmetry, C_{2v}, and all calculations reported here are performed using that point group. All calculations were performed using the Amsterdam Density Functional (ADF) package, version 2024.101;[34] full details are given in the Experimental Section. Using the Perdew, Burke, and Ernzerhof (PBE) functional,[35] we have located two quite distinct but closely spaced doublet states, $^2B_1$ and $^2A_1$, on the potential surface. Optimized bond lengths of both are compared to the experimental values in Table 1, and net spin densities of the two states are listed in Figure 3. The frontier orbital region of $[Cr_6@Sn_8Sb_8(en)_2]^{3-}$ is shown in Figure 4. In $^2B_1$ (referred to henceforth as the "Cr_6 radical state"), the unpaired electron is in the $3b_1$ orbital (Figure 4) localized on the Cr_6 core, while in $^2A_1$ (the "Sn radical state"), it is localized in $5a_1$, a linear combination of Sn−Sn bonding orbitals. Despite the very different localization of the unpaired electron, the Cr_6 and Sn radical states are very close in energy, the latter being more stable by only 0.03 eV at this level of theory. Given the approximations in our computational model (most notably the absence of K^+ counterions, the effect of which we model only approximately through the imposition of a continuum with a high dielectric constant), we consider this difference too small to be definitive. We therefore turn to a comparison with the available experimental evidence (both structural and spectroscopic) to identify the ground state. In the Sn radical state ($^2A_1$), the optimized structure of the $Cr_6@Sn_8Sb_8$ core retains almost perfect D_{4h} symmetry despite the presence of the en ligands, but the Cr−Cr and Sn−Sn bond lengths are shorter and longer, respectively, than the experimental values (Table 1). The Cr_6 radical state ($^2B_1$), in contrast, shows more significant deviations from D_{4h} symmetry with equatorial Cr−Cr bond lengths distributed over a range of ∼0.1 Å. We can trace this distortion to a first-order Jahn−Teller effect: the singly occupied molecular orbital (SOMO) in the $^2B_1$ state, $3b_1$, correlates with one component of a degenerate pair (the other being $6a_1$) in D_{4h} symmetry. The $^2A_1$ state, in contrast, correlates with a nondegenerate $^2B_{1g}$ state in the D_{4h} limit, so the Cr_6 core is not intrinsically unstable with respect to a first-order distortion. The nature and origin of the Jahn−Teller instability are discussed in more detail in the Supporting Information, Figure S8, but it suffices to note that the average bond lengths for the Cr_6 radical state offer a closer match to experiment, for both Cr−Cr and Sn−Sn bonds, than those for the Sn radical alternative. The structural differences between the two states are consistent with the transfer of an electron from a Cr−Cr bonding orbital ($3b_1$ in Figure 4) to one with a Sn−Sn bonding character ($5a_1$). The second piece of experimental evidence that we have at our disposal is the X-band EPR spectrum (measured at 95 K), which shows a broad isotropic signal centered on $g = 2.21$ (Figure 3). The computed g values for the $^2B_1$ state are 1.98, 2.02, and 2.20, the average of which, 2.09, is in reasonable accord with the experimental value (the distribution of values reflecting the distortions from perfect D_{4h} symmetry noted above). In contrast, the computed g tensor for the $^2A_1$ state is strongly axial, with principal values of 4.00, 2.06, and 2.05. We find no evidence of a signal around $g = 4$ in the spectrum, leading us to conclude that the Cr_6 radical state, $^2B_1$, is the more plausible candidate for the ground state despite the fact that it is calculated to be marginally less stable than the Sn radical alternative. We emphasize again that the energetic difference of 0.03 eV between the two states is well below the threshold that we would consider significant, given the approximations in our model.

The valence electron count on the Cr_6 core is a matter of some importance in the context of the wider comparison with the $Cr_6E_8(PR_3)_6$ family, all of which have a count of 20 on the formal Cr^{16+} core. To identify the corresponding count in $[Cr_6@Sn_8Sb_8(en)_2]^{3-}$, we first establish the charge state of the Sn_8Sb_8 ligand. The Sb_{12} unit in $[La@Sb_{12}]^{3-}$ is unambiguously Sb_{12}^{6-}, so each Sb_4 unit carries a net charge of −2. The Zintl−Klemm pseudoelement concept establishes an isolobal relationship between Sb_4^{2-} and $(Sn_2Sb_2)^{4-}$, which then suggests that the Sn_8Sb_8 ligand carries a formal charge of −16. This is the case in the Cr_6 radical state ($^2B_1$), where we can identify 44 occupied valence orbitals localized on the $(Sb_8Sn_8)^{3-}$ unit, up to and including $5a_1$ in Figure 4. Charge balance then requires that the Cr_6 core carries a charge of +13 and therefore a valence electron count of 23, three electrons more reduced than the formally 20-electron Cr_6^{16+} cores in $Cr_6E_8(PR_3)_6$ and $Cr_6E_8(CO)_6$. In the Sn radical state ($^2A_1$), in contrast, one electron is transferred from the $5a_1$ orbital to $3b_1$, leaving only 87 electrons on the $Sn_8Sb_8^{15-}$ unit and a compensating charge and valence electron count of +12 and 24, respectively, on the Cr_6 core. For the reasons set out in the previous paragraph, we favor the Cr_6 radical state as the most likely candidate for the ground state, but in either case, the electron count at the Cr_6 core is significantly higher than the characteristic value of 20 for $Cr_6E_8(PR_3)_6$.

Cotton and Haas first set out the basic molecular orbital framework of octahedral clusters in 1964,[36] and the Kohn−Sham molecular orbital array for a typical member of this family, $Cr_6Te_8(CO)_6$ (formally Cr_6^{16+}), is also shown in Figure 4. The 12 Cr−Cr bonding orbitals of the octahedron (one per edge) transform as $a_{1g} + e_g + t_{1u} + t_{2u} + t_{2g}$, all of which are occupied apart from $1e_g$, giving the total valence electron count of 20 noted above. In $[Mo_6Cl_{14}]^{2-}$, in contrast, the $1e_g$ orbital is also occupied, raising the count to 24, equating to a single 2-center-2-electron Mo−Mo bond per edge. The $1e_g$ orbital (Figure 4) is simultaneously M−M bonding and M−E antibonding (π^*), so its occupation will strengthen M−M bonding at the expense of ME bonding. Clearly, Mo−Mo bonding dominates in $[Mo_6Cl_{14}]^{2-}$ and other clusters of the heavier transition metals, where counts of 24 prevail, while M−E bonding is relatively more significant in the $Cr_6E_8L_6$ family, where counts of 20 are the norm. The most striking feature of the comparison of $Cr_6E_8(CO)_6$ with $[Cr_6@Sn_8Sb_8(en)_2]^{3-}$ shown in Figure 4 is that the $1e_g$ orbital is substantially stabilized (and split) in the latter, to the extent that the stable electron count is 23 rather than 20: Cr-ligand π bonding is clearly rather weaker than that in typical $Cr_6E_8L_6$ clusters, while Cr−Cr bonding is rather stronger. The weak Cr−Sb π bonding is reflected in the long Cr−Sb bonds (2.74−2.79 Å) compared to 2.65−2.67 Å for the Cr−Te bonds in $Cr_6Te_8(PEt_3)_6$.[37] We can trace the origin of the weak π bonding to the cyclic structure of the Zintl-ion ligand, which ties up precisely half of the 16 orbitals that would be available for π donation in the E_8 array in the Sn−Sb σ bonds.

CONCLUSIONS

In this paper, we have reported the synthesis of a new cluster, $[Cr_6@Sn_8Sb_8(en)_2]^{3-}$, containing an octahedral Cr_6 core encapsulated within a Sn_8Sb_8 Zintl-ion ligand. The remarkably short Cr−Cr bonds in the Cr_6 core mark this cluster out as being electronically quite distinct from members of the

https://doi.org/10.1021/jacs.5c00515
J. Am. Chem. Soc. 2025, 147, 24309−24316

$Cr_6E_8(PEt_3)_6$ family, where the Cr−Cr bond lengths are up to 0.3 Å longer. The stronger Cr−Cr bonding stems from a valence electron count of 23, three more than the typical count for the phosphine-terminated clusters, and in that sense, the cluster bears a closer resemblance to the heavier Mo_6, W_6, and Re_6 analogues where electron counts of 24 are typical. The fundamental differences in electron count can be traced to the rather unusual properties of the face-capping Sb atoms of the Sn_8Sb_8 "ligand", which have a reduced capacity to act as π donors compared to an array of 8 isolated chalcogenide ions.

EXPERIMENTAL SECTION

Synthesis. All manipulations and reactions were performed under a nitrogen atmosphere by using standard Schlenk or glovebox techniques. Ethylenediamine (Aldrich, 99%) and toluene (Aldrich, 99.8%) were freshly distilled from sodium/benzophenone. DMF (Aldrich, 99.8%) was distilled from CaH_2 under N_2 and stored under nitrogen prior to use. 18-crown-6 (1,4,7,10,13,16-Hexaoxacyclooctadecane, 98%) purchased from Sigma-Aldrich was dried in vacuum for 1 day prior to use. The precursor K_2SnSb was synthesized by fusing a mixture of the elements in a 2:1:1 ratio in a Nb tube at 900 °C for 2 days.[38] $CrCp_2$ was synthesized according to the reported literature preparation.[39]

Synthesis of {[K(18-C-6)]$_2$Cp}$_3${[Cr$_6$@Sn$_8$Sb$_8$(en)$_2$]}, 1. K_2SnSb (90 mg, 0.282 mmol) and 18-crown-6 (115 mg, 0.435 mmol) were dissolved in 2.5 mL of en and stirred at 50 °C for 0.5 h to yield a brown solution. $CrCp_2$ (26 mg, 0.143 mmol) was added slowly over 0.5 h, and then the mixture was stirred vigorously at room temperature for 3 h. The resulting brown solution was centrifuged and filtered with standard glass wool, then carefully layered with 3 mL of toluene. After 2 weeks, long black plate-like crystals of **1** formed in the test tube with approximately 21% yield (based on the amount of K_2SnSb used). The addition of PPh_3 does not alter the yield of **1** or lead to the formation of clusters in more oxidized states.[40]

Structural Characterization. Suitable single crystals of **1** were selected for X-ray diffraction analyses. Crystallographic data were collected on a Rigaku XtalAB Pro MM007 DW diffractometer with graphite monochromated Cu Kα radiation (λ = 1.54184 Å). Structures were solved using direct methods and then refined using SHELXL-2014 and Olex2 to convergence, in which all of the nonhydrogen atoms were refined anisotropically during the final cycles. All hydrogen atoms of the organic molecule were placed by geometrical considerations and were added to the structure factor calculation. Both compounds are air- and moisture-sensitive in solution and in the solid state. Crystallographic data is deposited in the Cambridge Crystallographic Database (CCDC), entry 2212805.

Electrospray Ionization Mass Spectrometry (ESI-MS). Electrospray ionization mass spectrometry (ESI-MS) was performed in negative-ion mode on an LTQ linear ion trap spectrometer by an Agilent Technologies ESI-TOF-MS(6230). The spray voltage was 5.48 kV, and the capillary temperature was kept at 300 °C. The capillary voltage was 30 V, and the sheath gas was maintained at 50 °C. The samples were made up inside a glovebox under an N_2 atmosphere and rapidly transferred to the spectrometer in an airtight syringe by direct infusion with a Harvard syringe pump at 0.2 mL/min.

Energy Dispersive X-ray (EDX) Spectroscopy. EDX analyses were performed by using a scanning electron microscope (FE-SEM, JEOL JSM-7800F, Japan). Data acquisition was performed with an acceleration voltage of 15 kV and an accumulation time of 60 s.

Electron Paramagnetic Resonance Spectroscopy. The EPR spectrum of a crystalline sample of **1** was collected at 94 K in the *Sharing of Apparatus Management Platform* at Nankai University. X-band measurements were performed with a Bruker-E580-10/12 spectrometer equipped with an FT/CW microwave bridge, a Flexline resonator, and an ESR-900 liquid helium cryostat. Nonsaturating conditions were found, with a microwave frequency of 9.3943 GHz, a microwave power of 47.43 mW, a modulation amplitude of 0.2 mT, a time constant of 50.00 ms, and a sweep rate of 300 s over 100 mT.

Computational Methods. All calculations described in this paper were performed with the Amsterdam Density Functional (ADF) package of program, version 2024.101.[34] The exchange-correlation functional proposed by Perdew, Burke, and Ernzerhof (PBE) was used throughout,[35] and scalar relativistic effects were introduced using the zeroth-order regular approximation (ZORA).[41] For all geometry optimizations, a triple-ζ quality basis set of Slater-type orbitals was used,[42] supplemented by two sets of polarization functions. Electrons up to and including 2p (Cr), 4p (Sn, Sb), and 1s (C, N, F) were treated using the frozen core approximation. The conductor-like screening model (COSMO) was applied to simulate the confined crystal environment in the experiment with a dielectric constant of 100.[43] The nature of the stationary points was determined by calculating the frequencies in the harmonic approximation. In the case of the $[Cr_6@Sn_8Sb_8(en)_2]^{3-}$ system, the analysis was complicated by the presence of the en ligands, which contain several single bonds about which rotation is almost barrierless. In the chosen conformation (with C_{2v} point symmetry), the $^2A_1$ state has two residual imaginary frequencies (60.5 and 55.4 $i$cm^{-1}) associated with torsions about the Cr−N bonds. The marginally less stable $^2B_1$ state also has two imaginary frequencies with similar characteritics at 61.1 and 56.3 $i$cm^{-1}, along with a third imaginary mode (649.8 $i$cm^{-1}). Attempts to eliminate this imaginary mode by removing all symmetry elements led to convergence on the more stable $^2A_1$ state, which necessarily transforms as the same representation in symmetries lower than C_{2v}.

ASSOCIATED CONTENT

Supporting Information

The Supporting Information is available free of charge at https://pubs.acs.org/doi/10.1021/jacs.5c00515.

Characterization data for **1**. Further details of computational analysis and optimized coordinates for all calculated species (PDF)

Accession Codes

Deposition Number 2212805 contains the supplementary crystallographic data for this paper. These data can be obtained free of charge via the joint Cambridge Crystallographic Data Centre (CCDC) and Fachinformationszentrum Karlsruhe Access Structures service.

AUTHOR INFORMATION

Corresponding Authors

John E. McGrady − *Department of Chemistry, University of Oxford, Oxford OX1 3QZ, U.K.;* orcid.org/0000-0002-8991-1921; Email: john.mcgrady@chem.ox.ac.uk

Zhong-Ming Sun − *State Key Laboratory of Elemento-Organic Chemistry, Tianjin Key Lab for Rare Earth Materials and Applications, School of Materials Science and Engineering, Nankai University, Tianjin 300350, China;* orcid.org/0000-0003-2894-6327; Email: sunlab@nankai.edu.cn

Authors

Wei-Xing Chen − *State Key Laboratory of Elemento-Organic Chemistry, Tianjin Key Lab for Rare Earth Materials and Applications, School of Materials Science and Engineering, Nankai University, Tianjin 300350, China*

Aidan Manley − *Department of Chemistry, University of Oxford, Oxford OX1 3QZ, U.K.*

Zi-Sheng Li − *Department of Chemistry, University of Oxford, Oxford OX1 3QZ, U.K.;* orcid.org/0000-0002-8545-9640

Complete contact information is available at:

https://pubs.acs.org/10.1021/jacs.5c00515

Author Contributions

[§]W.-X.C. and A.M. contributed equally.

Notes

The authors declare no competing financial interest.

■ ACKNOWLEDGMENTS

This work was supported by the National Natural Science Foundation of China (22425107, 22371140, and 92461303 to Z.-M.S.), the Natural Science Foundation of Tianjin City (No. 21JCZXJC00140), the China Postdoctoral Science Foundation under grant number 2024M761514, and the 111 project (B18030) from Ministry of Education China. A.M. acknowledges the EPSRC (UK) for a scholarship through the TMCS CDT Programme, grant number EP/L015722/1.

■ REFERENCES

(1) Frenking, G. Building a quintuple bond. *Science* **2005**, *310*, 796−797.
(2) McGrady, J. *Comprehensive Inorganic Chemistry II*, 2nd ed.; Reedijk, J.; Poeppelmeier, K., Eds.; Elsevier: Amsterdam, 2013; pp 321−340.
(3) Peligot, E. Sur un nouvel oxide de chrome. *C. R. Acad. Sci.* **1844**, *19*, 609−618.
(4) van Niekerk, J. N.; Scheoning, F. R. L. X-ray evidence for metal-to-metal bonds in cupric and chromous acetate. *Nature* **1953**, *171*, 36−37.
(5) Figgis, B. N.; Martin, R. L. Magnetic studies with copper(II) salts. Part I. Anomalous paramagnetism and δ-bonding in anhydrous and hydrated copper(II) acetates. *J. Chem. Soc.* **1956**, 3837−3846.
(6) Nguyen, T.; Sutton, A. D.; Brynda, M.; Fettinger, J. C.; Long, G. J.; Power, P. P. Synthesis of a stable compound with five-fold bonding between two chromium(I) centers. *Science* **2005**, *310*, 844−847.
(7) Wagner, F. R.; Noor, A.; Kempe, R. Ultrashort metal−metal distances and extreme bond orders. *Nat. Chem.* **2009**, *1*, 529−536.
(8) Bartholomew, A. K.; Juda, C. E.; Nessralla, J. N.; Lin, B.; Wang, S. G.; Chen, Y.-S.; Betley, T. A. Ligand-based control of single-site vs. multi-site reactivity by a trichromium cluster. *Angew. Chem., Int. Ed.* **2019**, *58*, 5687−5691.
(9) McGrady, J. E.; Weigend, F.; Dehnen, S. Electronic structure and bonding in endohedral Zintl clusters. *Chem. Soc. Rev.* **2022**, *51*, 628−649.
(10) Mayer, K.; Weßing, J.; Fässler, T. F.; Fischer, R. A. Intermetalloid clusters: molecules and solids in a dialogue. *Angew. Chem., Int. Ed.* **2018**, *57*, 14372−14393.
(11) Wilson, R. J.; Lichtenberger, N.; Weinert, B.; Dehnen, S. Intermetalloid and heterometallic clusters combining p-block (semi)-metals with d- or f−block metals. *Chem. Rev.* **2019**, *119*, 8506−8554.
(12) Zhou, B.; Denning, M. S.; Kays, D. L.; Goicoechea, J. M. Synthesis and isolation of $[Fe@Ge_{10}]^{3-}$: A pentagonal prismatic Zintl ion cage encapsulating an interstitial iron atom. *J. Am. Chem. Soc.* **2009**, *131*, 2802−2803.
(13) Espinoza-Quintero, G.; Duckworth, J. C. A.; Myers, W. K.; McGrady, J. E.; Goicoechea, J. M. Synthesis and characterization of $[Ru@Ge_{12}]^{3-}$: an endohedral 3-connected cluster. *J. Am. Chem. Soc.* **2014**, *136*, 1210−1213.
(14) Min, X.; Popov, I. A.; Pan, F.-X.; Li, L.-J.; Matito, E.; Sun, Z.-M.; Wang, L.-S.; Boldyrev, A. I. All-metal antiaromaticity in Sb_4-type lanthanocene anions. *Angew. Chem., Int. Ed.* **2016**, *55*, 5531−5535.
(15) Lichtenberger, N.; Wilson, R. J.; Eulenstein, A. R.; Massa, W.; Clérac, R.; Weigend, F.; Dehnen, S. Main group metal-actinide magnetic coupling and structural response upon U(4+) inclusion into Bi, Tl/Bi, or Pb/Bi cages. *J. Am. Chem. Soc.* **2016**, *138*, 9033−9036.
(16) Eulenstein, A. R.; Franzke, Y. J.; Lichtenberger, N.; Wilson, R. J.; Deubner, H. L.; Kraus, F.; Clérac, R.; Weigend, F.; Dehnen, S. Substantial π-aromaticity in the anionic heavy-metal cluster $[Th@Bi_{12}]^{4-}$. *Nat. Chem.* **2021**, *13*, 149−155.
(17) Lips, F.; Clérac, R.; Dehnen, S. $[Pd_3Sn_8Bi_6]^{4-}$: A 14-vertex Sn/Bi cluster embedding a Pd_3 triangle. *J. Am. Chem. Soc.* **2011**, *133*, 14168−14171.
(18) Chen, W.-X.; Tian, W.-J.; Li, Z.-S.; Wang, J.-J.; Muñoz-Castro, A.; Frenking, G.; Sun, Z.-M. Capturing aromatic Cr_5 pentagons in large main-group molecular cages. *Nat. Synth.* **2025**, *4*, 471−478.
(19) Hessen, B.; Siegrist, T.; Palstra, T.; Tanzler, S. M.; Steigerwald, M. L. Hexakis(triethylphosphine)octatelluridohexachromium and a molecule-based synthesis of chromium telluride, Cr_3Te_4. *Inorg. Chem.* **1993**, *32*, 5165−5169.
(20) Kamiguchi, S.; Imoto, H.; Saito, T.; Chihara, T. Syntheses, structures, FAB mass spectra, and magnetic properties of chromium chalcogenide cluster complexes $[Cr_6Se_8(PEt_3)_6]$, $[Cr_6Se_8(H)(PEt_3)_6]$, and $[Cr_6S_8(H)(PEt_3)_6]$. *Inorg. Chem.* **1998**, *37*, 6852−6857.
(21) Tsuge, K.; Imoto, H.; Saito, T. Syntheses, structures, and molecular-orbital calculations of chromium Chevrel-type cluster complexes $[Cr_6E_8(PR_3)_6]$ (E = S, PR_3 = PEt_3, PMe_3; E = Se, PR_3 = PEt_3, PMe_3, PMe_2Ph). *Bull. Chem. Soc. Jpn.* **1996**, *69*, 627−636.
(22) Saito, T.; Imoto, H. Chalcogenide cluster complexes of chromium, molybdenum, tungsten, and rhenium. *Bull. Chem. Soc. Jpn.* **1996**, *69*, 2403−2417.
(23) Gray, T. G. Hexanuclear and higher nuclearity clusters of the Groups 4 metals with stabilizing π-donor ligands. *Coord. Chem. Rev.* **2003**, *243*, 213−235.
(24) Fan, P.-D.; Deglmann, P.; Ahlrichs, R. Electron counts for face−bridged octahedral transition metal clusters. *Chem. - Eur. J.* **2002**, *8*, 1059−1067.
(25) Lin, Z.; D Williams, I. Structure and bonding in face- and edge-bridged octahedral transition metal clusters. *Polyhedron* **1996**, *15*, 3277−3287.
(26) Bügel, P.; Krummenacher, I.; Weigend, F.; Eichhöfer, A. Experimental and theoretical evidence for low-lying excited states in $[Cr_6E_8(PEt_3)_6]$ (E = S, Se, Te) cluster molecules. *Dalton Trans.* **2022**, *51*, 14568−14580.
(27) Yang, Y.-N.; Li, Z.-S.; Mondal, S.; Qiao, L.; Wang, C.-C.; Tian, W.-J.; Sun, Z.-M.; McGrady, J. E. Metal-metal bonds in Zintl clusters: Synthesis, structure and bonding in $[Fe_2Sn_4Bi_8]^{3-}$ and $[Cr_2Sb_{12}]^{3-}$. *Chin. Chem. Lett.* **2024**, *35*, No. 109048.
(28) Weigend, F.; Schrodt, C. Atom-type assignment in molecules and clusters by perturbation theory—A complement to X-ray structure analysis. *Chem. - Eur. J.* **2005**, *11*, 3559−3564.
(29) Lips, F.; Schellenberg, I.; Pöttgen, R.; Dehnen, S. The subtle influence of binary versus homoatomic Zintl ions: the phenyl-ligated trimetallic cage $[Sn_2Sb_5(ZnPh)_2]^{3-}$. *Chem. - Eur. J.* **2009**, *15*, 12968−12973.
(30) Cai, X.; Majumdar, S.; Fortman, G. C.; Koppaka, A.; Serafim, L.; Captain, B.; Temprado, M.; Hoff, C. D. Thermodynamic, kinetic, structural, and computational studies of the Ph_3Sn-H, $Ph_3Sn-SnPh_3$, and $Ph_3Sn-Cr(CO)_3C_5Me_5$ bond dissociation enthalpies. *Inorg. Chem.* **2016**, *55*, 10751−10766.
(31) Vránová, I.; Kremláček, V.; Erben, M.; Turek, J.; Jambor, R.; Ružička, A.; Alonso, M.; Dostál, L. A comparative study of the structure and bonding in heavier pnictinidene complexes (ArE)M-$(CO)_n$ (E = As, Sb and Bi; M = Cr, Mo, W and Fe). *Dalton Trans.* **2017**, *46*, 3556−3568.
(32) Kesanli, B.; Fettinger, J.; Eichhorn, B. The closo-$[Sn_9M(CO)_3]^{4-}$ Zintl ion clusters where M = Cr, Mo, W: two structural isomers and their dynamic behavior. *Chem. - Eur. J.* **2001**, *7*, 5277−5285.
(33) Charles, S.; Eichhorn, B. W.; Rheingold, A. L.; Bott, S. G. Synthesis, structure, and properties of the $[E_7M(CO)_3]^{3-}$ complexes where E = P, As, Sb and M = Cr, Mo, W. *J. Am. Chem. Soc.* **1994**, *116*, 8077−8086.
(34) te Velde, G.; Bickelhaupt, F. M.; Baerends, E. J.; Fonseca Guerra, C.; van Gisbergen, S. J. A.; Snijders, J. G.; Ziegler, T. Chemistry with ADF. *J. Comput. Chem.* **2001**, *22*, 931−967.

(35) Perdew, J. P.; Burke, K.; Ernzerhof, M. Generalized gradient approximation made simple. *Phys. Rev. Lett.* **1996**, *77*, 3865−3868.
(36) Cotton, F. A.; Haas, T. E. A molecular orbital treatment of the bonding in certain metal atom clusters. *Inorg. Chem.* **1964**, *3*, 10−17.
(37) Saito, T.; Yamamoto, N.; Nagase, T.; Tsuboi, T.; Kobayashi, K.; Yamagata, T.; Imoto, H.; Unoura, K. Molecular models of the superconducting Chevrel phases: syntheses and structures of $[Mo_6X_8(PEt_3)_6]$ and $[PPN][Mo_6X_8(PEt_3)_6]$ (X = S, Se; PPN = $(Ph_3P)_2N$). *Inorg. Chem.* **1990**, *29*, 764−770.
(38) Wilson, R. J.; Broeckaert, L.; Spitzer, F.; Weigend, F.; Dehnen, S. $[CuSn_5Sb_3]^{2-}]_2$: A dimer of inhomogeneous superatoms. *Angew. Chem., Int. Ed.* **2016**, *55*, 11775−11780.
(39) Spreer, L. O.; Shah, I. Evidence for a novel π-bonded aquo-organochromium(III) ion, $([\eta^5\text{-}(C_5H_5)Cr(OH_2)_n]^{2+}$. *Inorg. Chem.* **1981**, *20*, 4025−4027.
(40) Sevov, S. C.; Goicoechea, J. M. Chemistry of deltahedral Zintl ions. *Organometallics* **2006**, *25*, 5678−5692.
(41) van Lenthe, E.; Ehlers, A.; Baerends, E.-J. Geometry optimizations in the zero order regular approximation for relativistic effects. *J. Chem. Phys.* **1999**, *110*, 8943−8953.
(42) Van Lenthe, E.; Baerends, E. J. Optimized Slater-type basis sets for the elements 1−118. *J. Comput. Chem.* **2003**, *24*, 1142−1156.
(43) Klamt, A.; Schürmann, G. COSMO: a new approach to dielectric screening in solvents with explicit expressions for the screening energy and its gradient. *J. Chem. Soc., Perkin Trans.* **1993**, *2*, 799−805.

https://doi.org/10.1021/jacs.5c00515
J. Am. Chem. Soc. 2025, 147, 24309−24316